One-dimensional Ising ferromagnet $[(CH_3)_3NH]FeCl_3 \cdot 2H_2O$: Magnetic properties, crystal structure, and Mössbauer spectroscopy

R. E. Greeney and C. P. Landee*
Department of Physics, Clark University, Worcester, Massachusetts 01610
and Francis Bitter National Magnet Laboratory, Massachusetts Institute of Technology, Cambridge, Massachusetts 02139

J. H. Zhang and W. M. Reiff
Department of Chemistry, Northeastern University, Boston, Massachusetts 02115
(Received 26 July 1988; revised manuscript received 12 January 1989)

The crystal structure of $[(CH_3)_3NH]FeCl_3 \cdot 2H_2O$,FeTAC, has been determined and found to be isomorphous to that of the cobalt and nickel analogs, CoTAC and NiTAC. The structure consists of chains of bichloride-bridged Fe^{2+} ions extending along the b axis of the orthorhombic unit cell [space group *Pnma*, $a=16.711(3)$ Å, $b=7.361(1)$ Å, $c=8.140(1)$ Å, $R=0.0488$, $R_w=0.0674$]. These chains are linked into a two-dimensional (2D) network in the c direction by hydrogen bonding; the resulting planes are well isolated in the a direction by the organic molecules. The low-temperature magnetic susceptibilities are highly anisotropic with the greatest susceptibility along the b axis. Susceptibility data along b can be fit to the 1D Ising model with a small molecular-field correction giving a ferromagnetic intrachain exchange ($J_b/k=17.4$ K). The molecular-field correction shows the total interchain exchange to be negative and small ($z'J'/zJ \approx -2\times10^{-3}$), making FeTAC the most one-dimensional magnet of this series. Antiferromagnetic ordering is observed in both the susceptibility data and the Mössbauer spectra near 3.12 K. Analysis of both polycrystalline and single-crystal Mössbauer spectra show that V_{zz} is positive, corresponding to an orbital single (^5B) ground term based on the real d_{xy} orbital. This analysis also shows the easy axis of magnetization to lie in the ab plane. Low-field magnetization data show metamagnetic transitions when small fields are applied along the b axis. The metamagnetic phase diagram indicates the critical field is 90 Oe at $T=0$ K. High-field magnetization data up to 15 T indicate the presence of spin canting. Extraction of interchain exchange constants consistent with all the experimental data has not been possible. One possible description finds $z_cJ_c/k=-0.04$ K, with $z_aJ_a/k=0$ K by symmetry, making FeTAC an example of a rectangular 2D Ising system in the ordered state.

I. INTRODUCTION

Much information on the properties of low-dimensional magnetic systems has been obtained from studies on the series of compounds of the general formula $[(CH_3)_3NH]MX_3 \cdot 2H_2O$ (Refs. 1–16) (Tables I and II), where $X=$Cl, Br, and $M=$Mn, Fe, Co, Ni, and Cu. In this paper, we report on the structure, magnetic properties, and Mössbauer spectra of the ferrous chloride member of this series $[(CH_3)_3NH]FeCl_3 \cdot 2H_2O$, referred to as FeTAC hereafter. A preliminary report has been published previously.[17]

The members of this series are isostructural or nearly so (Table I). All are orthorhombic, space group *Pnma*, except for MnTAB and CuTAC, which are monoclinic, but deviate from orthorhombic symmetry by less than two degrees. Variation in lattice parameters between any two chloride compounds is 4.3% at the maximum and in most cases much less. All members are characterized by pronounced linear chain (1D) behavior and relatively large magnetic anisotropy (Table II). In most cases some degree of spin canting has been observed. Four of the six compounds are reported to be metamagnets and one shows a spin-flop transition. Given the similarities in structure and differences in anisotropy, along with the relative ease with which high quality single crystals can be grown, there is much potential for mixed phase studies combining compounds in this series.

Interest in FeTAC was further motivated by the research of Johnson and Bonner[18] on the thermodynamic properties of ferromagnetic linear chains. Their study examined the influence of exchange anisotropy and magnetic field upon the elementary excitations of Ising-Heisenberg ferromagnetic chains and predicted the existence of novel field dependencies for the magnetic specific heat and magnetic susceptibility. FeTAC is currently being used to examine these predictions.[19]

Other Fe^{2+} magnetic chains, particularly compounds of the family $AFeCl_3 \cdot 2Aq$ ($A=$Cs, Rb; Aq$=H_2O,D_2O$), have been studied extensively. Like FeTAC, these systems are Ising-type 1D magnets, which show canting and in some cases metamagnetic transitions.[20–23] In spite of the numerous studies done on these compounds, which have clearly characterized them as good 1D Ising systems, there has been a noticeable lack of susceptibility data. The data which have been reported[22,23] curiously fail to be described by the simple 1D Ising model which described CoTAC so thoroughly. In this paper we

TABLE I. Crystal parameters for members of the series $[(CH_3)_3NH]MX_3 \cdot 2H_2O$ (M=metal, X=halide).

	MnTAC	MnTAB	FeTAC	CoTAC	NiTAC	CuTAC
a (Å)	16.733	16.90	16.711	16.671	16.677	16.730
b (Å)	7.422	7.65	7.361	7.237	7.169	7.479
c (Å)	8.198	8.54	8.140	8.113	8.103	7.864
Unit cell	Orthorhombic	Monoclinic	Orthorhombic	Orthorhombic	Orthorhombic	Monoclinic
Space group	*Pnma*	$P2_1/m$	*Pnma*	*Pnma*	*Pnma*	$P2_1/c$
Canting		4°	≈30°	22°	21°	
Fold angle	16.20°		16.3°	15.58°	15.26°	
M—O bond c-axis angle	10.12°		12.7°	10.59°	11.40°	
Refs.	1,3,7,12	1,2,4	This work	8,9	11,12	16

characterize FeTAC in terms of this simple model, but not without some difficulty.

II. EXPERIMENTAL

A. Sample preparation

Samples of the pale lime green FeTAC were prepared by first dissolving iron powder in a 6M solution of HCl. Equimolar amounts of trimethylammonium chloride dissolved in water were added, and the solution slowly evaporated in a desiccator. Single crystals of up to several hundred milligrams could be obtained by careful slow evaporation of the solution. The largest crystals were usually obtained from seeded solutions. Most of the preparation and all the crystal growth was done in a nitrogen environment. In dry crystals the Fe^{2+} ions are only slightly prone to oxidation. Dampness and heat should be avoided in preparation and storage, as these factors greatly increase the rate of oxidation.

Crystals grow elongated along the b (chain) axis, which is readily identified. Since crystals are often bounded by {201} faces, the a and c axes can sometimes be determined by visual inspection. A polarizing microscope was used to check the orientation of the crystallographic axes and to check for twinning and defects in the crystals. Crystal orientation can also be checked by locating the cleavage plane which is parallel to the bc plane. The chemical formula of FeTAC has been verified by commercial chemical analysis.[24]

B. X-ray structural determination

X-ray diffraction data collections were performed at Washington State University by R. D. Willett on a Nicolet $R3m/E$ diffractometer system.[25] The structures were solved using direct methods within the version 4.1 SHELXTL structure solution package.[26] The empirical absorption correction (μ=22.67 cm^{-1}) was applied for the room-temperature data collection. Initial positions for the atoms were approximated by the positions reported for CoTAC.[8] The structure was refined by adjusting the atomic positions and thermal parameters which were anisotropic for all nonhydrogen atoms. A least-squares refinement on 85 parameters achieved a final R value of 0.0488 with R_w=0.0674. The largest peak on the final difference map was 0.6 $e/Å^3$ near Cl(1). Atomic coordinates and thermal parameters are given in Table III, and bond distances and angles in Table IV.

C. Magnetic measurements

Magnetic measurements were made using a PAR Model 155 Vibrating Sample Magnetometer and a custom helium cryostat. Temperature and field measurements were made using a calibrated carbon glass resistance ther-

TABLE II. Magnetic parameters for members of the series $[(CH_3)_3NH]MX_3 \cdot 2H_2O$ (M=metal, X=halide).

	MnTAC	MnTAB	FeTAC	CoTAC	NiTAC	CuTAC
J/k (K)	−0.36	−0.41	17.4	13.8	14.0	0.85
$Z'J'/k$ (K)	−0.55	−0.74	−0.04	0.28	0.13	
$Z''J''/k$ (K)			0.00	−0.032	−0.024	−0.024
D/k (K)	0.144	0.515		4.9	−3.7	
E/k (K)	0.048	0.035			2.0	
T_c (K)	0.98	1.56	3.12	4.18	3.67	0.16
Special feature	Spin-flop	Metamagnet	Metamagnet	Metamagnet	Metamagnet	
Refs.	1,5,6	1,2,4,6	This work	8,9	11,12	13–15

TABLE III. Fractional coordinates and equivalent isotropic thermal parameters for $[(CH_3)_3NH]FeCl_3 \cdot 2H_2O$.

Atom	x	y	z	U_{eq}[a]
Fe	0	0	0	0.0169(5)
Cl(1)	−0.099 94(8)	0.25	0.0011(2)	0.0211(6)
Cl(2)	0.099 96(8)	0.25	−0.0666(2)	0.0218(5)
Cl(3)	−0.087 75(9)	0.25	0.4985(2)	0.0250(6)
O	0.0224(2)	0.0375(4)	0.2532(4)	0.0231(10)
N	0.1835(3)	0.25	0.3087(8)	0.024(2)
C(1)	0.1672(5)	0.25	0.4846(8)	0.034(2)
C(2)	0.2269(3)	0.0831(8)	0.2552(7)	0.037(2)

[a]The equivalent isotropic U is defined as one-third of the trace of the orthogonalized U_{ij} tensor.

mometer and Hall probe, respectively. A detailed description of the experimental apparatus has appeared elsewhere.[27] The background moment as a function of angle and field (there is little or no temperature dependence) was measured independently and is significant only when measuring small moments. Diamagnetic and demagnetization corrections have been made. The most accurate measurements for the large easy axis susceptibility were obtained using a crystal shaped into an ellipsoid. High-field measurements, up to 150 kOe, were taken at the Francis Bitter National Magnet Laboratory using a Foner-type vibrating sample magnetometer.

Susceptibility measurements (defined as $\partial M/\partial H$ in the limit of small H) were performed in the smallest possible field, and always in regions where the magnetization is linear with field. Below the ordering temperature, data along the easy axis were taken in the minimum remnant field of the magnet, about 10 Oe.

Final alignment of the crystals was done by applying a magnetic field and searching for extrema in the moment as a function of angle of orientation at a temperature well above the ordering temperature. The large degree of anisotropy allowed the axes to be located to an accuracy of better than ±2°.

TABLE IV. Bond lengths and bond angles for $[(CH_3)_3NH]FeCl_3 \cdot 2H_2O$ (and $FeCl_2 \cdot 2H_2O$).

Bond	Length (Å)	
Fe—Cl(1)	2.485(1)	[2.488(3)]
Fe—Cl(2)	2.544(1)	[2.542(3)]
Fe—O	2.113(4)	[2.075(5)]
Bond	**Angle (deg)**	
Cl(1)—Fe—Cl(2)	84.6(1)	[87.4(2)]
Cl(1)—Fe—Cl(2a)	95.4(1)	
Cl(1)—Fe—O	91.1(2)	(90)
Cl(2)—Fe—O	89.8(2)	(90)
O—Fe—Cl(1a)	88.9(2)	(90)
O—Fe—Cl(2a)	90.2(2)	(90)
Fe—Cl(1)—Fe(a)	95.5(1)	(92.6)
Fe—Cl(2)—Fe(a)	92.7(1)	
Dihedral fold	16.3	(0)

Near the ordering temperature, the susceptibility along the easy axis (b axis) is 3 orders of magnitude larger than the susceptibilities along a or c. A misalignment of as little as 2° will mask the true behavior of χ_a and χ_c. Great care was taken in mounting and aligning the crystals to ensure that no component of the b-axis susceptibility was measured.

D. Mössbauer spectroscopy

Mössbauer spectra of polycrystalline samples of FeTAC have been measured using a conventional constant acceleration spectrometer operated in horizontal geometry. The source was ^{57}Co (100 μCi) diffused into a Rh matrix held at room temperature. The temperature of the sample was varied in a flow-type helium cryostat between about 1.4 K and room temperature and was determined using either a calibrated silicon diode and/or vapor pressure thermometry. Some spectra were also measured in a magnetic field smaller than 3 kOe, produced by a small electromagnet perpendicular to the direction of the gamma ray. Single-crystal spectra were measured for thin single crystals or a mosaic grouping.

III. RESULTS

A. Crystal structure description

FeTAC has been found to be isostructural with several other compounds in the TAC series (Table I). It is orthorhombic, space group *Pnma*, with lattice parameters: $a=16.711(3)$ Å, $b=7.361(1)$ Å, and $c=8.140(1)$ Å. There are four formula units per unit cell.

Each Fe^{2+} ion sits at the center of a distorted octahedron formed by four chlorines and the two oxygens from *trans*-H_2O groups (Fig. 1). The plane formed by the four chlorines is distorted slightly from a perfect square into a parallelogram in which the iron ion is located at the center. The octahedral is compressed axially along the Fe—O bonds, and the Fe—O bond vector is tilted 1.1° from the normal to the plane. Relevant distances and bond angles are given in Table IV.

The octahedra form chains along the b axis by sharing edges; each Fe^{2+} ion is therefore bibridged to the next ferrous ion by two chlorines (Fig. 1). The dihedral fold angle (between adjacent $FeCl_4^{2-}$ planes) is 16.3°, slightly

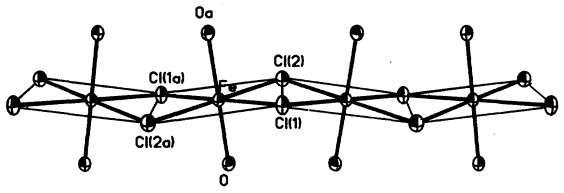

FIG. 1. Chains of edge-sharing octahedra shown projected onto the *bc* plane. The chains run along the *b* axis. The Fe—O bonds make an angle of 12.7° with the *c* axis. Normals to adjacent chloride planes are tilted alternatively 8.15° from the *c* axis.

larger than the value of the equivalent angles found in CoTAC and NiTAC (Table I). The distance between adjacent Fe^{2+} ions along the chain is 3.680 Å. Adjacent octahedra are mirror images due to the presence of a mirror plane perpendicular to *b* which passes through the centers of the two bridging chlorines. There also exists a twofold screw axis parallel to *b* which permits the existence of spin canting, as discussed in Sec. IV B.

Hydrogen bonding between water molecules and lattice chloride anions, Cl(3), situated between the chains in the *c* direction (Fig. 2), joins the chains of octahedra along *b* into sheets in the *bc* plane. The repeat distance between the chains along *c* is simply one unit-cell translation (8.140 Å). This hydrogen bonding creates an interchain exchange pathway, Fe—O—H · · · Cl · · · H—O—Fe, which is long and relatively weak. Previous studies of the interchain exchange in the *M*TAC family have shown it to be only about one percent as strong as the intrachain exchange (Table II).

The chains are positioned in the *bc* plane such that the Fe—O bonds are tilted 12.7° above or below the *c* axis (Fig. 3). Each chain within the same *bc* layer is identical. Water molecules are located alternately and below the *bc* plane at a distance of ±0.38 Å (Fig. 3).

The planes are stacked normal to the *a* axis, separated

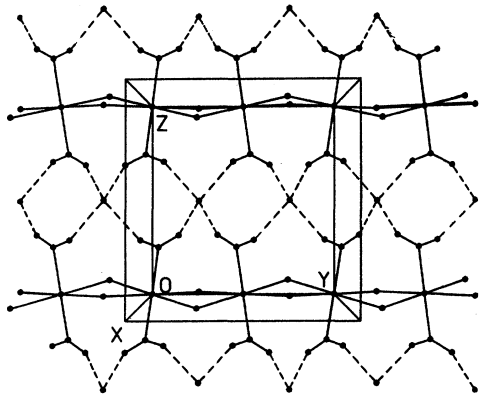

FIG. 2. Adjacent chains shown projected onto the *bc* plane. Dashed lines indicate interchain hydrogen bonding between water molecules and the interchain chloride ions Cl(3). All iron atoms lie in a plane. All other atoms lie slightly above or below this plane.

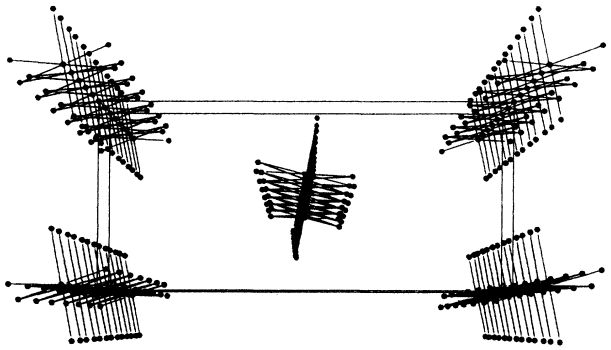

FIG. 3. Three-dimensional representation of the unit cell of $[(CH_3)_3NH]FeCl_3 \cdot 2H_2O$. The chains along the *b* direction (into the page) extend beyond the unit cell. The *c* axis is vertical and the *a* axis is horizontal. Not all atoms are shown to emphasize the one-dimensional and two-dimensional character of the compound.

by a distance of *a*/2 (8.356 Å). Adjacent planes are related by two symmetry operations; an *n* glide perpendicular to the *a* axis and an *a* glide perpendicular to the *c* axis (Fig. 3). Within a single *bc* plane, all the Fe—O bond vectors are rotated out of the plane in the same sense, whereas the sense of rotation is reversed in adjacent planes. The planes are separated by the large trimethylammonium groups which provide no clear superexchange pathway; the exchange between the magnetic layers appears to be primarily dipolar. In previous studies on related compounds (Table II), this exchange has been found to be 5 to 10 times weaker than the exchange between the chains.

B. Magnetic susceptibility

The susceptibility of FeTAC has been measured along all three crystallographic axes from 1.4 to 300 K. At 300 K the susceptibilities along all three axes are the same within 6.0%, $\chi_b = 1.02\chi_a = 1.06\chi_c$. As the temperature is lowered, the three susceptibilities gradually separate, χ_c remaining the lowest and χ_b remaining the highest. By 100 K the three principal susceptibilities are clearly different: $\chi_b = 1.13\chi_a = 1.33\chi_c$. Figure 4 shows the three susceptibilities plotted as the log of susceptibility versus temperature between 1.4 and 40 K. The semilog plot allows the three susceptibilities to be conveniently shown on one plot, demonstrating the clear Ising-type behavior of this compound. At 3.18(2) K, χ_b reaches its maximum value of 100 emu/mol, more than 1200 times the value of either χ_a or χ_c. Below 3.18 K χ_b drops rapidly toward zero, decreasing more than 3 orders of magnitude by 1.4 K. The abrupt change in slope and rapid decrease in the susceptibility is taken to be an indication of 3D antiferromagnetic ordering. The critical temperature (T_c), taken to be the temperature at which the derivative of the susceptibility, $\partial\chi_b/\partial T$, shows a maximum, is 3.12(2) K.[28]

The susceptibilities along the *a* and *c* axes are similar to each other in behavior and magnitude (Fig. 5). χ_a has a maximum value of 0.157 emu/mol at 13.5(5) K. After

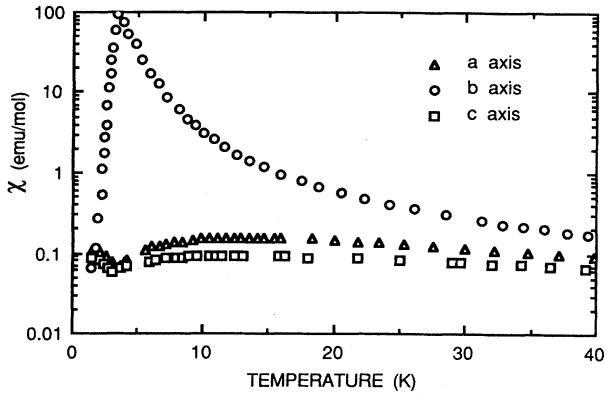

FIG. 4. The magnetic susceptibilities of FeTAC measured along all three axes plotted on a semilogarithmic scale.

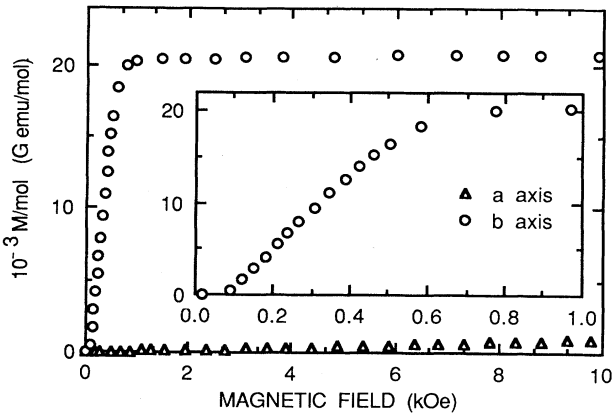

FIG. 6. Magnetization of FeTAC measured along the a and b axes at $T=2.1$ K in fields up to 10 kOe. The rapid magnetization along b is indicative of a metamagnetic phase transition. A detail of the b axis magnetization is shown in the inset.

reaching its maximum, it falls steadily to 0.067 emu/mol at 3.2 K, then rises to 0.101 emu/mol at 2.05 K, below which it remains constant. χ_c lies below χ_a throughout the entire temperature range studied. χ_c reaches its maximum value of 0.092 emu/mol at 12.5(1.0) K and drops to a minimum of 0.0574 emu/mol just below the ordering temperature at 3.0 K, rising again to the constant value of 0.0862 emu/mol at 1.6 K.

C. Magnetization

Magnetization studies have been made at a variety of temperatures both above and below T_c along all three axes. Measurements taken in fields up to 10 kOe were made at Clark University using a 12-in electromagnet. The high-field data in fields up to 150 kOe were collected at $T=1.37$ K at the Francis Bitter National Laboratory. The results along the a and b axes at $T=2.1$ K are shown in Fig. 6. The magnetization along the chain axis is gradual and linear with field up to approximately 40 Oe, at which point the magnetic moment begins to change rapidly. Between 40 Oe and 600 Oe the moment has increased by a factor of 5000 to a value of 18 400 emu/mol. By 1.0 kOe the moment is already 98% of its value at 10 kOe (Fig. 6) or 93% of its value at 150 kOe (Fig. 7).

This steplike behavior is characteristic of a metamagnetic phase transition. The critical field (H_c), defined as the field for which $\partial M/\partial H_i$ has its maximum value (H_i = internal field), marks the boundary between the ordered antiferromagnetic and paramagnetic regions. H_c varies with temperature (Fig. 8) as does the sharpness of the "step." The metamagnetic transition is theoretically first order below the tricritical point,[29] but the observed transition is spread out over a range of applied field (Fig. 6); this is a result of the demagnetizing effect of the rapid magnetization near the critical field. When the moment is plotted as a function of applied field (inset, Fig. 6), the transition spans 500 Oe. When the moment is plotted as a function of internal field (H_i), a much sharper transition is seen.[30] Since the sample is not a perfect ellipsoid, the internal field is not uniform throughout the sample

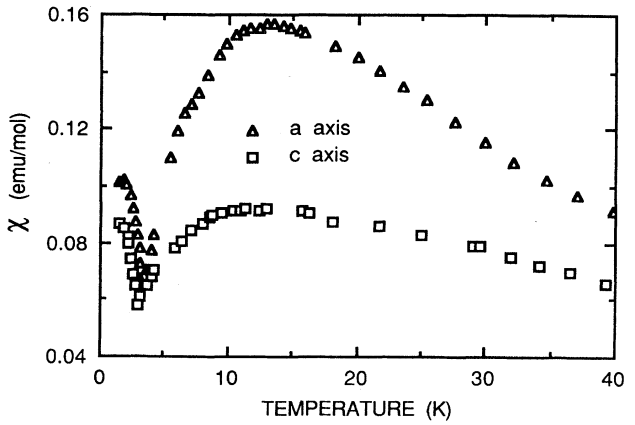

FIG. 5. The low-temperature magnetic susceptibilities χ_a and χ_c for FeTAC plotted vs temperature.

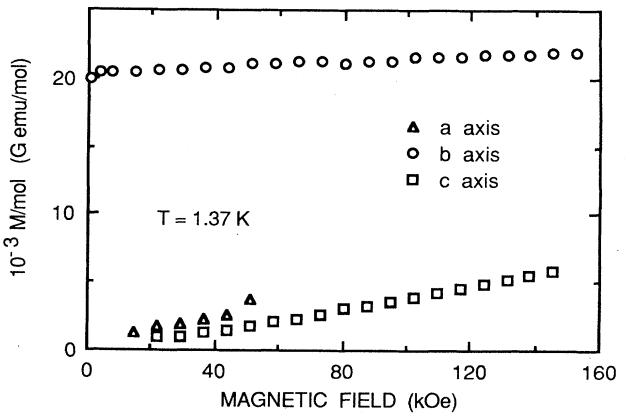

FIG. 7. High-field magnetization of FeTAC measured along all three axes. The data was collected at $T=1.37$ K.

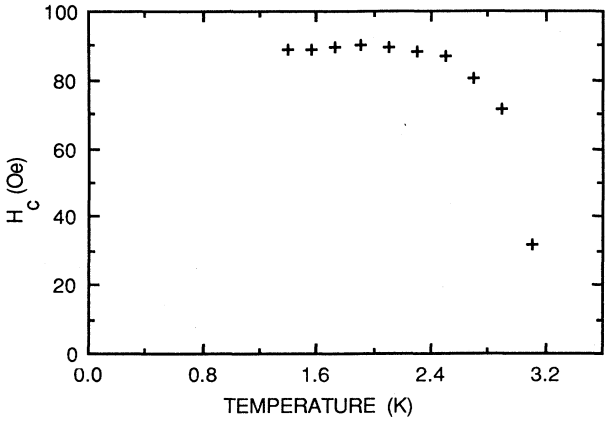

FIG. 8. The metamagnetic phase diagram for FeTAC with the magnetic field applied parallel to the b axis. The internal field, H_i, has been calculated from the applied field H_a using the relation $H_i = H_a - NM$, where N is the demagnetization factor. The value of the critical field extrapolated to 0 K is 90 Oe.

and some smearing of the transition remains.

The a and c magnetization curves are similar to each other in their behavior. Both are approximately linear from lowest to highest field. Figure 6 does not show the low-field c-axis data which lie slightly below the a-axis set. The high-field magnetization data for both the a and c axes are shown in Fig. 7, but the a-axis data stops at about 50 kOe; at this value of the field, the sample was pulled from the sample rod by the large torque.

D. Mössbauer

The Mössbauer spectra for FeTAC prove helpful in understanding aspects of the three-dimensional magnetic ground state. We consider spectra for the paramagnetic phase first, then those of the ordered state.

The spectrum of a polycrystalline sample at ambient temperature corresponds to a well-resolved quadrupole doublet typical of high-spin iron (II) (isomer shifts and quadrupole splittings are given in Table V). The spectrum of FeTAC shows a temperature dependence that is remarkably similar to that of $FeCl_2 \cdot 2H_2O$ for which detailed analysis[31,32] of the temperature dependence using the approach of Ingalls[33] indicates a (low-symmetry ligand field component) splitting of the t_{2_g} manifold of the order of 500 cm^{-1}. The limiting value of the quadrupole interaction, ≈ 2.7 mm/s at 77 K, suggests an orbital singlet ground state. In particular, in view of the local coordination chromophore (a tetragonally compressed *trans*-$FeCl_4O_2$ environment), one predicts an orbital singlet ground state. In tetragonal symmetry this corresponds to a ^5B ground term based primarily on the real d_{xy} orbital. For this ground-state wave function, the expectation value of the operator for the principal component of the electric-field-gradient (EFG) tensor is $-(\frac{4}{7})q\langle r^{-3}\rangle$. This is positive for electron occupation and leads to a positive electric quadrupole coupling constant, since the quadrupole moment of iron-57 is positive. The sign of this interaction is important in understanding the orientation of the internal hyperfine field of the ordered state relative to the principal axis of the electric-field-gradient tensor, and is considered subsequently.

TABLE V. Isomer shifts and quadrupole splittings for the Mössbauer spectra of $[(CH_3)_3NH]FeCl_3 \cdot 2H_2O$.

T (K)	Isomer shifts (δ)[a]	Quadrupole splittings (ΔE_Q)
280	1.17	2.34
200	1.22	2.55
120	1.26	2.71
78	1.27	2.73
10	1.34	2.72

[a]Relative to natural iron metal.

The prediction of a positive electric quadrupole coupling constant is confirmed by the single-crystal Mössbauer spectra obtained in the paramagnetic phase. A spectrum is shown in Fig. 9 at ambient temperature, corresponding to the orientation of a single crystal such that the direction of gamma-ray propagation is parallel to the orthorhombic unit-cell c axis. The local fourfold axis (O—Fe—O axis) is nearly along this direction. Thus, one has essentially a single-crystal spectrum with the direction of gamma-ray propagation parallel to the principal axis of the EFG tensor. Under this condition—if, in fact, the principal component of the electric-field-gradient tensor is positive—then one expects from the angular components of the selection rules

$$|I=\tfrac{1}{2}, m_I=\pm\tfrac{1}{2}\rangle \rightarrow |I=\tfrac{3}{2}, m_I=\pm\tfrac{1}{2}\rangle ,$$

$$\text{intensity} \propto \tfrac{5}{3} - \cos^2(\beta) ,$$

$$|I=\tfrac{1}{2}, m_I=\pm\tfrac{1}{2}\rangle \rightarrow |I=\tfrac{3}{2}, m_I=\pm\tfrac{3}{2}\rangle ,$$

$$\text{intensity} \propto 1 + \cos^2(\beta) ,$$

(β is the angle from the axis of symmetry) that the

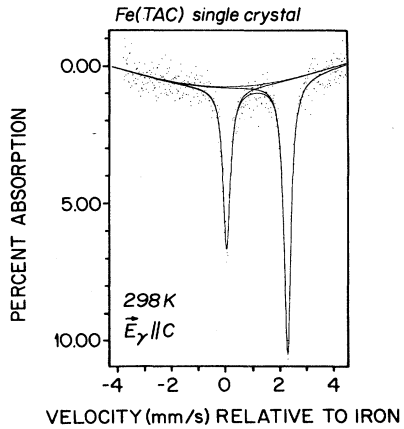

FIG. 9. Mössbauer spectra of an oriented single-crystal sample of FeTAC taken in zero field at 298 K. The gamma rays propagate parallel to the c axis.

lower-energy transition (I_L) will be of lower intensity than the higher-energy gamma-ray transition (I_H), the transition at higher positive velocity. The reverse situation obtains if the field gradient tensor is negative. The theoretical ratio for an infinitely thin absorber with perfect alignment under the circumstance of a positive principal component of the electric-field-gradient tensor is $I_H/I_L=3/1$. Our value, 1.6/1, is somewhat different from this limit, owing, in part, to thickness broadening and imperfect orientation (V_{zz} is tilted some 13° away from the c axis). However, it is clear from the spectrum and from the fit that the amplitude and overall intensity of the lower-energy transition is less than those of the higher, thus confirming V_{zz} to be positive, as anticipated. A similar result was obtained for $FeCl_2 \cdot 2H_2O$ from single-crystal measurements;[31] however, broadening effects resulted in an even larger deviation ($I_H/I_L=1.5/1$) from the theoretical value of the intensity ratio.

Some Mössbauer spectra (polycrystalline sample) showing the three-dimensional magnetic ordering of FeTAC are given in Figs. 10 and 11. It is seen that there is an abrupt transition to a three-dimensionally ordered state just below 3.2 K, in good agreement with the magnetic susceptibility measurements. The spectrum at 3.5 K shows initial broadening above T_c. It is possible that this broadening is the result of single-ion slow paramagnetic relaxation phenomena—a negative zero-field splitting of the single-ion spin quintet manifold leading to a slowly relaxing $m_s=\pm 2$ ground Kramers doublet. Such broadening can also be the result of soliton effects (moving domain boundaries in the present context) in a one-dimensional magnet just above the critical ordering temperature.[34] These possibilities can be unequivocally distinguished only by determination of a considerable number of spectra of spectra above T_c and detailed line width analysis, aspects beyond the scope of the present work.

FeTAC readily magnetizes for very small applied fields, as seen in the spectrum taken at 3.15 K in a transverse applied field of 300 Oe (bottom of Fig. 10). The resulting spectrum has a value of internal hyperfine field and degree of resolution that are comparable to the zero-field spectrum taken at 1.64 K (bottom of Fig. 11). The limiting spectrum at 1.64 K gives clear evidence of a large quadrupolar shift and perturbation of the hyperfine split spectrum; in fact, the spectrum is reminiscent of many ferrous systems in which eight transitions are actually present ($\Delta m_1=\pm 2$ transitions weakly allowed). It is clear, however, that all these transitions cannot be

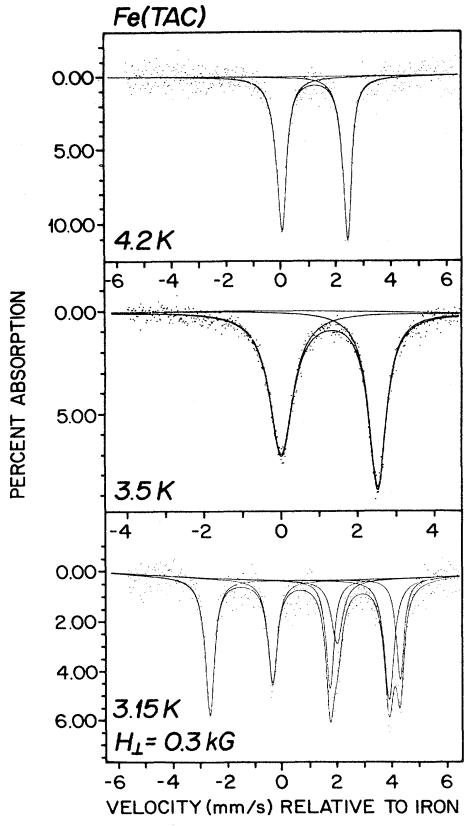

FIG. 10. Mössbauer spectra of a powdered sample of FeTAC taken at $T=4.2$, 3.5, and 3.15 K (top to bottom). The spectra taken at the two higher temperatures were taken in zero field; the spectra taken at 3.15 was collected in an applied field of 0.3 kOe. The orientation of the field was perpendicular to the direction of propagation of the gamma rays.

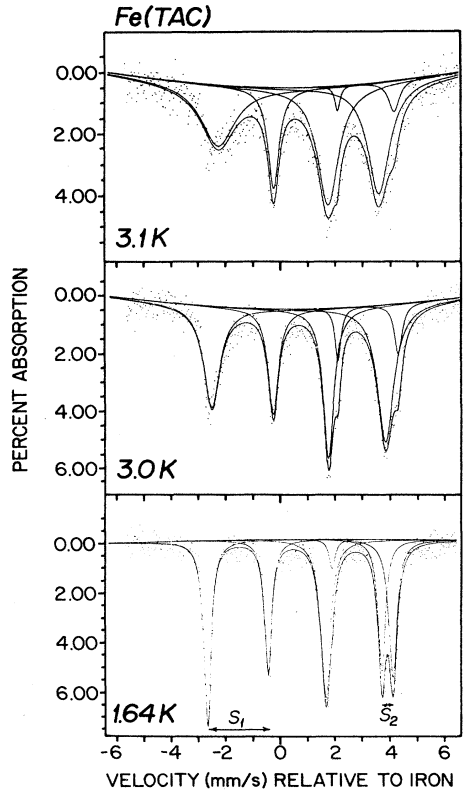

FIG. 11. Mössbauer spectra of a powdered sample of FeTAC taken in zero field at 3.1, 3.0, and 1.64 K (top to bottom). S_1 and S_2 define the quadrupolar shifts described in Sec. III D.

resolved, and we have not tried to fit the spectra for eight transitions. In any event, the quadrupolar shift can readily be determined directly from the spectrum as is, and it is equal to the difference s_1-s_2, where s_1 and s_2 are the splittings shown in Fig. 12. For an axially symmetric EFG tensor, the quadrupolar shift is related to the quadrupole splitting, ΔE, of the paramagnetic phase by the equation

$$s_1-s_2=(-\Delta E)(3\cos^2\theta-1)\ ,$$

where θ is the angle between the principal axis of the electric-field-gradient tensor (V_{zz}) and the internal hyperfine field; it is therefore also the direction of the easy axis of magnetization for the ordered state. Since V_{zz} is positive, one can calculate θ from the combined interaction spectrum at 1.64 K using measured values for the difference s_1-s_2 and ΔE from the paramagnetic phase. The value for θ found by this calculation is 20° different from 90° (either 70° or 110°).

The crystallographic data (Sec. III A) indicate that the O—Fe—O direction (presumably the direction of the principal component of the electric field gradient) is tilted approximately 13° away from the orthorhombic unit-cell c axis by a rotation about the b axis. Consequently, one would expect that the angle θ between the principal axis of the EFG and the bulk easy axis (the b axis) would remain the angle between the Fe—O bonds and the b axis, i.e., 90°. The fact that the angle is found to be 20° different from this value we attribute to the presence of spin canting in the chains. While the b axis is the easy axis in the bulk, it is not the local easy axis at any site. A full discussion is given in Sec. IV B.

Single-crystal spectra determined in the magnetically ordered temperature region confirm the basic model of moments along the b axis, normal to the Fe—O bonds. Figure 12 shows one such spectrum ($T=1.43$ K) with the direction of gamma-ray propagation parallel to the c axis and hence nearly parallel to the principal axis of the electric-field-gradient tensor. The angular components of the selection rules for the gamma-ray transitions for magnetic dipole splitting are such that one has $\sin^2\theta$ dependence for the $\Delta m_I=0$ transitions.[35] This dependence would mean that one should have *enhancement* of these transitions for the orientation shown in Fig. 13 if, in fact, the internal hyperfine field and the easy axis lie in the ab plane. Comparison of the single-crystal spectrum to the lowest-temperature powder spectrum (bottom of Fig. 12) shows that this is the case (see arrows). The theoretical limiting hyperfine intensity patterns are 3:2:1::1:2:3 for the (thin, random) polycrystalline powder sample, while the intensities have the theoretical ratio 3:4:1::1:4:3 for a thin and perfectly oriented single crystal with an internal field perpendicular to E_γ. Again owing to thickness broadening effects and considerable overlap of the higher-energy $\Delta m_I=0$ transition (transition 5) with a $\Delta m_I=1$ transition (transition 6), one does not achieve the full theoretical consistent with the orientation of the local hyperfine field as concluded from the analysis of the powder spectra as well as analysis of the single-crystal susceptibilities.

The Mössbauer spectroscopy behavior for the paramagnetic and ordered states of FeTAC are remarkably similar to those of $FeCl_2\cdot 2H_2O$,[31] which exhibits a similar enhancement. The primary differences between the two materials are (1) slightly different unit cells, the dichloride being monoclinic but nearly orthorhombic, while FeTAC is rigorously orthorhombic and, more importantly, (2) the large difference in magnetic ordering temperature. The ordering temperature for $FeCl_2\cdot 2H_2O$ is 23 K while FeTAC orders at 3.12 K. This large difference in the Néel temperatures is due to the significant interchain dilution effect resulting from the presence of the bulky tertiary alkylammonium ions. A quantitative discussion of the difference is presented in Sec. IV D.

The limiting internal hyperfine fields for $FeCl_2\cdot 2H_2O$ and FeTAC are also similar with values of 240 and 200 kOe, respectively. These values are somewhat below the expected value of 440 kOe due to a Fermi contact contribution for four unpaired spins, that is, $S=2$ for high-spin iron(II). The reduced value is in part undoubtedly the result of a large orbital contribution, H_L, to the internal hyperfine field which generally opposes the Fermi contact

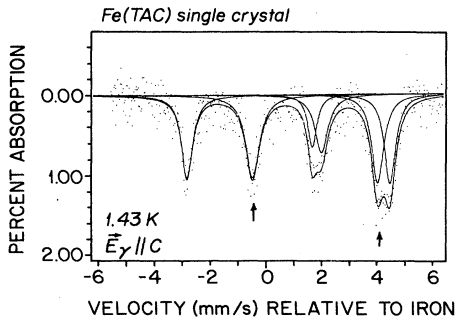

FIG. 12. Mössbauer spectra of an oriented single-crystal sample of FeTAC taken in zero field at 1.43 K. The gamma rays propagate parallel to the c axis.

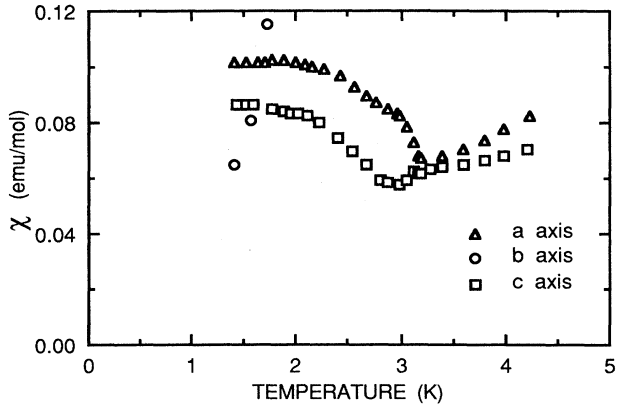

FIG. 13. Low-temperature magnetic susceptibilities measured along all three axes showing the behavior of $\chi_\parallel$ (b axis) and $\chi_\perp$ (a and c axes).

contribution. Other effects that can reduce the internal field are covalency delocalization and a factor peculiar to low-dimensional systems, zero-point spin reduction.[36] However, it is very difficult to separate all these effects for a system of this type.

IV. DISCUSSION

A. Ordering temperature

The critical temperature (T_c) has been determined from the susceptibility to be 3.12(2) K. The ordering temperature lies slightly below T_{max} (3.18 K), the temperature at which χ_b reaches its absolute maximum. The close proximity of T_c and T_{max} has been observed in the analogous compounds CoTAC (Ref. 9) and NiTAC (Ref. 12). This value of T_c is consistent with both the Mössbauer results (Figs. 10 and 11) and the metamagnetic phase diagram (Fig. 8). Determination of T_c through these techniques is considerably less precise.

B. Spin orientation and canting

The Ising-type nature of FeTAC, with the b axis as the easy axis, is clearly evident in both the magnetization data (Figs. 6 and 7) and the susceptibilities (Fig. 4). The application of magnetic fields parallel to the chain axis nearly brings M_b to saturation in fields of only several kilo-oersteds. However, when a field is applied parallel to the a or the c axis, the Ising anisotropy renders it difficult to bend the spins away from the b axis into the ac plane (Fig. 7). The magnetization curves are approximately linear from lowest to highest field, as expected for fields applied perpendicular to an Ising moment. Extrapolating these magnetization curves to the saturation value, we find the anisotropy field is approximately 400 kOe along a and 600 kOe along c.

The susceptibility data are also consistent with the model that b is the easy axis. χ_b decreases rapidly toward zero as the temperature approaches zero below the ordering temperature, behavior consistent with a parallel susceptibility of an ordered antiferromagnet. Both χ_a and χ_c go to constant values as the temperature approaches zero, behaving like perpendicular susceptibilities (Fig. 13). If spin canting is present, χ_b would not be a true $\chi_\parallel$, but rather a mixture of $\chi_\parallel$ and $\chi_\perp$. Thus χ_b would eventually reach a nonzero constant value, but no such limiting behavior is observed down to the lowest temperatures measured, 1.37 K. A quantitative description of this effect will be made later in the paper.

The high-field magnetization data (Fig. 7) eliminates from consideration an alternate spin alignment. The initial report on FeTAC (Ref. 17) analyzed the data as arising from antiferromagnetic chains with the bulk easy axis parallel to the a axis. The large moments along the b axis were explained by the presence of a large amount of spin canting in the b direction, similar to the structure observed in $RbFeCl_3 \cdot 2H_2O$.[20–22] The high-field magnetization study done subsequent to the preliminary publication eliminates the possibility that the spins lie along the a axis canted toward b (Fig. 7). When a field is applied along b the moment rapidly goes to a large value. By 1 kOe the moment is larger by a factor of 2.5 than the corresponding moment seen in $RbFeCl_3 \cdot 2H_2O$ at a field of 14 kOe.[19]

The crystallographic b axis is therefore established as the bulk easy axis in FeTAC, but the existence of canting in which the spins are tilted alternately $\pm\phi$ on either side of the b axis is still allowed by the twofold screw axis parallel to b. Such canting is a frequent occurrence in low-symmetry ferrous compounds such as $RbFeCl_3 \cdot 2H_2O$ and its cesium analog.[20] We now argue that the Mössbauer data, when compared to the data for the analogous compound $FeCl_2 \cdot 2H_2O$, imply that such canting must be present.

The crystal structure of $FeCl_2 \cdot 2H_2O$ (space group $C2/m$) consists of chains of edge-sharing $FeCl_4O_2$ octahedra extended along the c axis; the chains are held together by hydrogen bonds.[37] The two identical chains per unit cell are related by the centering operation. The local geometries about the iron ion are very similar in both $FeCl_2 \cdot 2H_2O$ and FeTAC (Table IV). Both consist of a plane of four chlorines with the water molecules nearly normal to the plane; in FeTAC the Cl(1)—Fe—O angle is 91.1° while it is 90° by symmetry for the dichloride. The bond lengths are nearly identical for the two compounds: Fe—Cl(1)=2.485 Å for FeTAC and 2.488 Å for $FeCl_2 \cdot 2H_2O$. An important distinction related to the magnetic structure is found in the number of distinct iron sites: The dichloride contains one site per unit cell while FeTAC contains two, related by the 2_1 screw axis parallel to b. This permits the tilting of the octahedra by ±8.15° in FeTAC; no such tilting exists in $FeCl_2 \cdot 2H_2O$.

The Mössbauer studies of the dichloride[31] showed the internal magnetic field to lie in the plane of the chlorides, as discussed in Sec. III D. Single-crystal susceptibility measurements[38] located the easy axis pointing along the direction of the shortest iron-chloride bond, Fe—Cl(1). Since each octahedra is identical, the local easy axes are parallel. The ferromagnetic exchange within the chains offers no competition to the orientation of the spins along the local axes; no canting is possible.

The individual $FeCl_4O_2$ octahedra are nearly identical in FeTAC and the dichloride; in addition, the similarity of the Mössbauer spectra of the two compounds has already been commented upon. We therefore make the assumption that the local crystal fields in the two compounds are similar and that the local easy axis of magnetization will be found along the Fe—Cl(1) bond in FeTAC as well. Spin canting is therefore introduced by the screw axis. The local Fe—Cl(1) axes of the two Fe^{2+} ions within each chain are not parallel (Fig. 1) but rather tilted alternately by approximately 45° away from the b axis. Since the plane of the chlorines is tilted by ≈13° away from the ab plane (Fig. 3), the local axes have small components along the crystallographic c axis as well as along the a and b axes. The dihedral fold of ±8.15° by adjacent chloride planes introduces an additional component of the local Fe—Cl(1) axis along c. In summary, in the absence of exchange interactions, we would expect the local easy magnetic axes to have a large, uncanted component along the chain axis b, and a significant cant-

ed component along the a axis, with a relatively small [on the order of sin(13°)] canted component along the c axis.

The ferromagnetic exchange within the chains will tend to align the moments parallel, bringing the moments away from their local easy axes. The actual amount of canting in the system consequently depends on the relative strengths of the exchange fields and local anisotropy fields. The exchange strength within the chains has been determined to be 17.4 K with a g factor along the chain direction of 7.5 (see Sec. IV D). This exchange strength has been converted to an effective field using the molecular field relation $H_{ex}=2zJS/g\mu_\beta$ with an effective spin value of $\frac{1}{2}$, and leads to a value of $=140$ kOe for H_{ex}. If the local anisotropy field is taken to equal the limiting local hyperfine field of 200 kOe obtained from the Mössbauer spectra, it is seen that the two fields are comparable. The exchange field will not be able to pull the spins into a parallel alignment, and canting along the a axis on the order of $\pm 30°$ will persist; a significantly smaller canting along the c axis will also be present.

The presence of such canting is consistent with the Mössbauer powder spectra. As discussed in Sec. III D, the quadrupolar shifts indicate the angle between the principle axis of the EFG and the local easy axis is 20° different from 90°. Such a difference is a natural consequence of the moments being pulled parallel to the b axis and out of the $FeCl_4^{2-}$ planes by the exchange interaction.

The absence of saturation in the b axis high-field magnetization data (Fig. 7) is also consistent with the presence of such spin canting. The magnetic moment rapidly approaches a state of near saturation when a field less than 1 kOe is applied parallel to the b axis, inducing the metamagnetic transition. However, the moment continues to increase steadily out to the largest applied fields. Raising the field from 1 to 150 kOe increases M_b by 6.4%. If due to canting alone and not thermal excitations, this small change in moment would correspond to a canting angle of at least 21°. The effect of finite temperatures upon the magnetization of a $S=\frac{1}{2}$ Ising ferromagnetic chain has been calculated[30] using the expression of Chalupa and Giri.[39] These results show that the magnetization at 1.37 K should be fully saturated in a field of only 10 Oe. Since the maximum applied field is 1.5×10^4 times larger than this value, the effect of thermal excitations is completely negligible; the continued increase in magnetization beyond 1 kOe must be due to spin canting.

The canting in FeTAC is hidden, whereas in CoTAC (Ref. 9) and NiTAC (Ref. 12) overt canting is present. The magnetic structure of CoTAC consists of ferromagnetic chains along b, merged into ferromagnetic layers in the bc plane by exchange through the waters and lattice chloride ions.[10] The moments lie in the ac plane and point nearly along the Co—O bond, being therefore tilted by about 10° towards the a axis. Adjacent planes are coupled antiferromagnetically with the c axis the bulk easy axis, but the canting along a is in the same sense in every plane; there is hence an uncompensated weak moment along a. In contrast, no net moment is seen in FeTAC along any of the three crystallographic axes in the ordered state.

C. One-dimensional interactions

The quantitative analysis of the data begins by describing the behavior of this system as a one-dimensional Ising system. The interaction Hamiltonian for this model is written as

$$H=-2J_b\sum_i (S_i^z S_{i+1}^z - g\mu_\beta H S_i^z)\ . \tag{1}$$

The two possible eigenvalues of S_i^z equal $\pm\frac{1}{2}$. The sum is taken over all pairs $\langle i,i+1\rangle$ along the b direction only. Calculation of the susceptibility from this Hamiltonian yields two expressions depending on the direction of the applied field, parallel or perpendicular to the z axis. These two expressions are[40]

$$\chi_\parallel=(C_\parallel/T)\exp(J_b/kT)\ , \tag{2}$$

$$\chi_\perp=(C_\perp/|J_b/k|)[\tanh|J_b/2kT| + |J_b/2kT|\operatorname{sech}^2(J_b/2kT)]\ , \tag{3}$$

where $C_\parallel$ and $C_\perp$ are the corresponding Curie constants defined as

$$C_{\parallel,\perp}=N(g_{\parallel,\perp})^2(\mu_\beta)^2/4k \tag{4}$$

for an effective $S=\frac{1}{2}$ system.

This expression does not take into account any spin canting. If spin canting is present, the local easy axis at each Fe^{2+} site is canted from the b axis by $\pm\phi$. A field applied along the b axis will have components both parallel and perpendicular to the true local easy axis. In that case χ_b is a mixture of $\chi_\parallel$ and $\chi_\perp$ according to the expression

$$\chi_b=\chi_\parallel\cos^2(\phi)+\chi_\perp\sin^2(\phi)\ . \tag{5}$$

Expecting ϕ to be about 20° means $\sin^2(\phi)$ is about 0.1. Since $\chi_\perp \ll \chi_\parallel$ (Fig. 4), χ_b can be well approximated to the expression for $\chi_\parallel$. In this case g_b and not $g_\parallel$ is measured.

A convenient graphical representation of Eq. (2) for the parallel susceptibility can facilitate the analysis of Ising chain systems:

$$\ln(\chi_\parallel T)=(J_b/k)T^{-1}+\ln(C_\parallel)\ . \tag{6}$$

A plot of $\chi_\parallel T$ versus T^{-1} on semilog paper gives a straight line for the theoretical model. The slope of the line is proportional to the exchange strength along the chain (J_b/k) and the y-axis intercept is equal to $C_\parallel$, the Curie constant for the easy direction. We refer to this plot as an Ising plot.

In Fig. 14, the Ising plots of both CoTAC and FeTAC are compared. Both systems show regions of good (linear) 1D behavior. In the case of CoTAC the linear region extends to $\frac{1}{40}$ K^{-1}, whereas in FeTAC significant deviations from ideal linear behavior end at about $\frac{1}{20}$ K^{-1}. The Ising-type 1D behavior extending over a broader temperature region for CoTAC compared to FeTAC implies that the excited-state doublets lie relatively higher above the ground state for the cobalt compound. The Is-

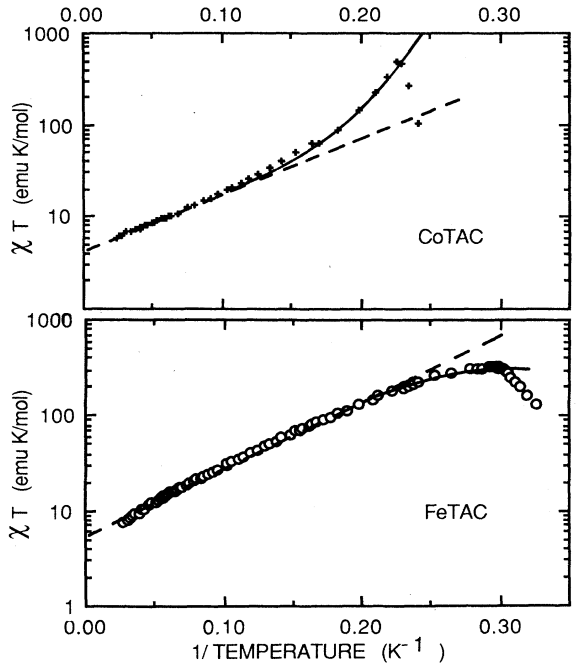

FIG. 14. Semilogarithmic plot of χT vs T^{-1} for FeTAC and CoTAC referred to as an Ising plot (see text). The dashed lines indicate the susceptibilities predicted for a pure 1D Ising ferromagnet with the magnetic field parallel to the easy axis [Eqs. (2) and (6)]. The solid lines represent the predictions of the same model with a molecular-field correction added [Eq. (7)]. The corresponding parameters are found in the text.

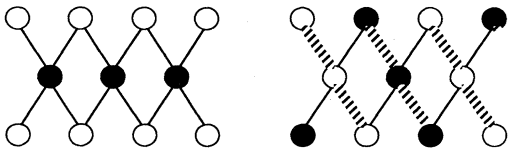

FIG. 15. Diagram showing two proposed models for the magnetic structure in FeTAC. The drawings represent projections of the FeTAC structure onto the *ac* plane; the *c* axis is horizontal and the *a* axis is vertical. Open circles correspond to ferromagnetic chains with the moments into the page; solid circles represent ferromagnetic chains with moments out of the page. The left drawing represents the CoTAC model. The exchange in the *c* direction is ferromagnetic, leading to ferromagnetic planes; exchange in the *a* direction is antiferromagnetic (represented by solid lines). The right drawing represents the Onsager model in which the exchange along *c* is antiferromagnetic. The *bc* planes are therefore antiferromagnetic. The exchange between layers is consequently zero by symmetry, since every metal ion is connected identically to two oppositely aligned moments.

ing plots of both compounds are quite linear until a temperature of $\frac{1}{2}T_c$ is reached, at which point deviations from the Ising model become significant. The most striking and important difference between the two plots occurs here. CoTAC deviates from the 1D model in a positive sense (curving upwards), indicating that the dominant interchain exchange is ferromagnetic, whereas FeTAC deviates from the model in a negative sense, implying that the dominant interchain exchange is antiferromagnetic. These features will be discussed in detail in the next section. For both compounds, the transition to the state of long-range order appears as a sharp break in the Ising plot at $1/T_c$.

The FeTAC data have been fit to the expression for $\chi_\parallel$ with the best fit obtained when the temperature region is restricted to the interval between 6 and 18 K. Lower temperatures cannot be included as the Ising plot of the data begins to curve downward. The result of this fit finds the intrachain exchange parameter $J_b/k=16.6(1)$ K and the Curie constant $C_b=5.52(4)$ emu K/mol. The largest difference between the calculated value of χ_b and the experimental value is $+2\%$. Although these errors are small they are systematic, and some rounding of the data can be seen.

It is important to note that the data for both CoTAC and FeTAC presented in Fig. 15 were collected under identical experimental conditions using the vibrating sample magnetometer (VSM) with small fields (on the order of 10–15 Oe) applied parallel to the easy axes of the samples. The data for CoTAC were measured in our laboratory to insure that the use of the VSM did not create anomalous results. The shape of the CoTAC crystal was not smooth; the estimated demagnetization factor was not as carefully determined as in the case of FeTAC. The fit of the CoTAC data to Eq. (2) gave the intrachain magnetic exchange parameter $J_b/k=15.2(1)$ K and the Curie constant $C=4.65(3)$ emu K/mol. The value of the exchange constant is in excellent agreement with that found by Losee *et al.*[8] but about 8% higher than the value determined by Groenendijk and van Duyneveldt.[9] The value for the Curie constant lies between the values determined in the previous two studies. We conclude that the VSM technique is valid for these materials and that the downward curvature of the Ising plot for FeTAC is therefore intrinsic.

The susceptibility data of FeTAC, taken with a field applied perpendicular to the bulk easy axis, shows a peak value in the susceptibility, for both H parallel to a and to c. Qualitatively, this is the behavior expected for a $\chi_\perp$ in a 1D Ising system. Fitting this data to the 1D Ising expression for $\chi_\perp$ [Eq. (3)] gives the result that $J_b/k=32.0(2)$ K, $C_a=4.18(2)$ emu K/mol for $\mathbf{H}\|a$ and $J_b/k=33.0(1.0)$ K, $C_c=2.58(6)$ emu K/mol for $\mathbf{H}\|c$. In both cases the quality of the fit is good. The relative difference between theory and experiment is better than 1% for all data points along a (10–30 K), and better than 4% for all data points along c (8–25 K). A detailed discussion of the inconsistency between the exchange constants obtained from the $\chi_\parallel$ and $\chi_\perp$ results appears at the end of Sec. IV D.

D. Interchain interactions

As seen in other members of the TAC family, interactions between the chains in both the a and c directions

lead to deviations from ideal 1D behavior and ultimately induce a transition to long-range order. The deviation from 1D behavior can be characterized by introducing a mean-field correction to the ideal 1D Ising model. The corrected susceptibility is given by the following expression:[41]

$$\chi_{MF}=\chi_{1D}(1-z'J'\chi_{1D}/2Ck)^{-1}\ , \tag{7}$$

where χ_{1D} is the ideal 1D susceptibility, and $z'J'/k$ is the total effective interchain magnetic exchange, $z'J'/k=z_aJ_a/k+z_cJ_c/k$. The exchange through the hydrogen bonding network in the c direction, J_c, has been found to be 5 to 10 times larger than the exchange between the layers, J_a, in both CoTAC (Ref. 9) and NiTAC (Ref. 12).

Fitting the χ_b data between 3.2 and 18 K to this expression yields the following results: $J_b/k=17.40(5)$ K, $C_b=5.26(5)$ K, and $z'J'/k=-0.0810(4)$ K. The values of the parameters are independent of the range of temperatures included in the fit, provided the lower temperature does not extend to T_c and the upper temperature does not exceed 20 K. The exchange energy (J_b/k) and the Curie constant (C_b) are not sensitive to small changes in N_b (the demagnetization factor along b) and are reported with a precision of $\pm1\%$. The exchange energy between the chains ($z'J'/k$) which characterizes the curvature of the Ising plot is quite sensitive to N_b; a change of $\pm5\%$ in N_b results in a shift of $\pm10\%$ in the value obtained for $z'J'/k$. Even allowing for this amount of uncertainty in the demagnetization factor, the value of $z'J'/k$ is unmistakably negative.

The fitting procedure described in the above paragraph ignored the hidden spin canting present in FeTAC; we have found that use of the more complete analysis, based on Eq. (5), did not change the main conclusions. The molecular-field-corrected expression for the canted susceptibility expression is a function of five variables (J, $g_\parallel$, $g_\perp$, the canting angle ϕ, and $z'J'$) which are highly correlated; use of all five as free parameters leads to unphysical results. If only data in the linear region of the Ising plot (6–20 K) were included, $g_\perp$ was found to be zero and ϕ undefined. Including the data at lower temperatures leads to a high correlation in the values of ϕ, $g_\parallel$, $z'J'$, and $g_\perp$. The value reported for J is not affected by the range of fit or the presence of canting, although $g_\parallel$ increases as the canting angle becomes larger; this is the necessary response to keep the same susceptibility when the component of $\chi_\parallel$ becomes smaller. The value for $z'J'=-0.081$ K is based on a canting angle of 0°; increasing ϕ decreases the magnitude of $z'J'$, so the value reported is an upper limit.

in contrast to the FeTAC result, the sum of the interchange exchange interaction in CoTAC has been reported[9] to be $z'J'/k=+0.26$ K, a positive value more than 3 times larger than the value found for FeTAC. Not only has the sign of the interchain interactions reversed in FeTAC, but a considerably greater degree of one-dimensional isolation occurs. This can be appreciated by a comparison of both the ordering temperatures (T_c) and the intrachain exchange energies (J_b/k) for FeTAC and CoTAC. Although the intrachain exchange energy of FeTAC ($J_b/k=17.4$ K) is 26% higher than in CoTAC ($J_b/k=13.8$ K),[9] its ordering temperature of 3.12 K is 25% lower [T_c(CoTAC)=4.18 K]. The critical ratio (kT_c/J) is therefore 0.179 for FeTAC and 0.302 for CoTAC, clearly indicating improvement in one dimensionality for the ferrous compound. The quantitative assessment of the improvement depends on the model used to determine the dependence of T_c upon the ratio J'/J.

There are two possibilities for the signs of the interchain interactions in FeTAC, under the proviso that the net J' is negative. The first possibility assigns z_cJ_c to be positive, leaving z_aJ_a to be negative. The ordered state therefore consists of ferromagnetic bc planes, antiferromagnetically coupled along a. This is the same combination of signs of exchange constants found in CoTAC and will be referred to as the CoTAC model. There is an important difference between CoTAC and FeTAC, however. In CoTAC the net interchain interaction $|z'J'/k|$ is positive, causing upward deviations of the Ising plot until the critical temperature is reached. The lattice dimensionality crossover pattern for CoTAC is therefore 1D ferromagnet to 2D ferromagnet to 3D antiferromagnet. In FeTAC, the Ising plot curves down, signifying that the antiferromagnetic interactions, J_a, between chains in the corners and center of the unit cell dominate (Fig. 15); the interactions in the a direction must therefore be larger than the interactions within the planes along c. The crossover pattern for FeTAC becomes 1D ferromagnet to 3D antiferromagnet.

The second possibility for the interchain exchange in FeTAC assigns J_c to be negative. In this case the exchange in the a direction cannot be determined, since any sign or value for J_a results in the same decoupled spin arrangement (Fig. 15). The chain in the center of the unit cell is coupled by identical exchange to the chains in the corners of the cell which are oriented in opposite directions. The net exchange in the a direction z_aJ_a/k is identically zero. Under these conditions $z'J'/k=z_cJ_c/k$. This model therefore proposes a 2D system of the independent antiferromagnetic Ising planes and will be called the Onsager model.

We choose between the two models by an analysis of the interchain exchange constants. The values obtained in this process are listed in Table VI. A value for the antiferromagnetic exchange strength J_{af} can be extracted from the magnetic phase diagram using the mean-field result:

$$-2z_{af}J_{af}S^2=g\mu_\beta SH_{cr}(0)\ . \tag{8}$$

Here $H_{cr}(0)$ is the metamagnetic critical field at $T=0$ K, determined to be 90 Oe by an extrapolation of the data in Fig. 8. Using $g_b=7.49$ ($C_b=5.26$) results in $z_{af}J_{af}/k=-0.0447$ K. For the Onsager model, in which $z_aJ_a=0$, $z_cJ_c/k=z_{af}J_{af}/k=-0.0447$ K, which is a value approximately one-half that obtained from the fit to the b axis susceptibility. A more troublesome inconsistency appears for the CoTAC model, in which J_a is antiferromagnetic and larger in magnitude than the ferromagnetic J_c. For this case $z_{af}J_{af}/k=z_aJ_a/k$

TABLE VI. Exchange constants in FeTAC and CoTAC.

$Z'J'/k$ (1D MF)[a]	$Z_{af}J_{af}/k$ $[H_c(0)]$[b]	$Z_{af}J_{af}/k$ (Onsager)[c]	$\lvert Z'J'/k\rvert$ (CN)[d]	J_b/k	Z_aJ_a/k	Z_cJ_c/k
			CoTAC			
0.26 K	−0.032 K	NA	0.308 K	13.8 K	−0.032 K	0.28 K
			FeTAC			
−0.081 K	−0.045 K	−0.047 K	0.024 K	17.4 K	−0.045 K[e]	<0.04 K[e]
					0.00 K[f]	−0.045 K[f]

[a]Value derived from the molecular field correction to the 1D $\chi_{\parallel}$, Eq. (7).
[b]Value derived from the molecular field expression for the metamagnetic critical field extrapolated to 0 K, Eq. (8).
[c]Value derived from the Onsager solution to the 2D rectangular Ising model, Eq. (9).
[d]Value derived from the Chalupa-Novotny expression for the critical temperature of coupled Ising chains, Eq. (11).
[e]CoTAC model: $J_a<0$; $J_c>0$ (3D antiferromagnet).
[f]Onsager model: $J_a=0$; $J_c<0$ (2D antiferromagnet).

$=-0.0447$ K; it is impossible for the net exchange $z'J'/k=z_aJ_a/k+z_cJ_c/k$ to equal the susceptibility result $z'J'/k=-0.081$ K for any positive value of J_c.

For the two-dimensional Onsager model, an independent estimate of J_c can be obtained. Onsager's expression[42] for the ordering temperature of a 2D rectangular Ising system is

$$[\sinh(J/kT_c)][\sinh(J'/kT)]=1\ , \tag{9}$$

where J and J' correspond to the exchange constants in the two orthogonal directions. Since $T_c=3.12$ K and $J/k=J_b/k=17.4$ K are known, $J'/k=J_c/k$ can be determined from Eq. (9) to be $|J_c/k|=0.0236$ K. Taking $z_c=2$ yields the result $z_cJ_c/k=-0.047$ K, in good agreement with the result for the metamagnetic phase diagram.

The sensitivity of the critical temperature to the values of the interchain exchange constants has been evaluated previously by Chalupa and Navotny (CN).[43] They considered a CoTAC-like system in which ferromagnetic Ising chains (exchange constant K) are coupled in one direction by a ferromagnetic interaction J_F and in the third direction by an antiferromagnetic interaction J_A. Both J_F and J_A are absolute magnitudes. Exact expressions are used for correlations within the chains, whereas the coupling through J_F and J_A is done in the mean-field approximation. They obtain an expression for the critical temperature in the presence of a field,

$$T_c(H)=2K/\ln[T_c/(J_F+J_A)(1-m^2)^{3/2}]\ , \tag{10}$$

where m is the staggered magnetization. In the limit of zero field, m goes to zero and the expression simplifies. Substituting $J_B/k=2K$, $|z_cJ_c/k|=2J_F$, $|z_aJ_a/k|=2J_A$, and rearranging the expression to a more convenient form yields

$$|z_cJ_c/k|+|z_aJ_a/k|=2T_c/\exp(J_b/kT)\ . \tag{11}$$

Substituting the proper values of T_c and J_b/k for both FeTAC and CoTAC produces the result that $|z_cJ_c/k|+|z_aJ_a/k|$ is equal to 0.308 K for CoTAC and 0.0236 K for FeTAC. In the case of CoTAC this is in excellent agreement with the published result[9] of 0.312 K. In the case of FeTAC the result is a factor of 2 lower than either the Onsager result or the metamagnetic result, and a factor of 3 lower than the mean-field Ising plot result. In any case, it is clear that the sum of the interchain exchange constants in FeTAC is reduced by at least a factor of 4 and possibly by as much as a factor of 12 from their values in CoTAC.

A list of the exchange strengths derived from the above procedures for both CoTAC and FeTAC appears in Table VI. We conclude that the most reliable value for the antiferromagnetic exchange between the chains in FeTAC has a value $z_{af}J_{af}/k=-0.045$ K, as obtained from the metamagnetic critical field. This value is consistent with the value for exchange coupling strength between chains in the 2D Ising model, Eq. (9), and therefore consistent with the Onsager model for FeTAC. The CoTAC model of ferromagnetic planes coupled antiferromagnetically is only consistent if the ferromagnetic exchange J_c becomes very small. Both models are inconsistent by a factor of 2 with the value of $z'J'/k=-0.081$ K obtained from the molecular-field correction to the $\chi_{\parallel}$ data, Eq. (7); however, that value is the least reliable since it was obtained under the assumption of zero canting and is highly sensitive to demagnetization corrections. In either case, the ratio $|z'J'/k|/|z_bJ_b/k|=1.3\times10^{-3}$; makes FeTAC an order of magnitude more isolated than CoTAC.

What accounts for the large reduction in the interchain exchange in FeTAC? A comparison of the magnetic parameters for the TAC family members in Table II shows that the interchain interaction in FeTAC is a factor of 10 smaller than for most of the other compounds and a factor of 3 smaller than the next smallest, NiTAC. The net interchain interaction for FeTAC is comparable to the secondary J' in other compounds, caused by dipolar interactions between the ferromagnetic planes. The answer does not appear to lie in any structural anomalies; investigation of Table I shows that FeTAC is a well-behaved member of the TAC family, with lattice parameters, bond distances, and fold angles that are consistent with the values found for other members.

We believe the small value of J' in FeTAC is due to the specific magnetic orbital occupied by the magnetic electron of the ferrous ion. As discussed in Sec. III D, the Mössbauer spectra are indicative of a single electron occupation of the d_{xy} orbital, lying in the plane of the four chloride ions surrounding the iron. Little magnetic electron density will overlap with the oxygen in the axial position; consequently, there will be only a slight superexchange pathway between chains along the water molecules and lattice chloride, Cl(3), Fig. 2. This pathway is significant in other members of the TAC family, leading to exchange values for J_c approximately one percent that of J_b in FeTAC; the lack of magnetic electron density in this pathway reduces J_c to about 0.1% of J_b. The superexchange and dipolar contributions to the interchain interaction are therefore comparable in FeTAC.

We now address the problem of fitting the susceptibility data along all three axes to a consistent set of parameters. The values of J_b/k derived from fitting χ_a and χ_b to the expression for $\chi_\perp$ [Eq. (3)] are almost a factor of 2 greater than the value of 17.4 K determined from the previously discussed fit to χ_b. However, the result $J_b/k = 17.4$ K, obtained from the $\chi_\parallel$ fits, is taken to be more accurate. Given the ordering temperature of 3.12 K and a value of $J_b = 32$ K, the model of CN [Eq. (11)] indicates a total interchain exchange of 0.000 22 K. This is an unreasonably small number, more than 2 orders of magnitude below that predicted by the metamagnetic field data.

Taking the value of $J_b/k = 17.4$ K as correct, the peak in the perpendicular susceptibilities should appear at about 7 K. It is unknown why the experimentally observed peak occurs at about 13 K. This temperature is low enough to be well within the 1D Ising regime and yet high enough that the effects of 2D or 3D interactions should be absent. Numerous attempts to resolve this inconsistency have been made by trying to fit χ_a and χ_c to an expression which includes canting [Eq. (5)] and/or an interchain molecular field correction [Eq. (7)]. Without exception, the inclusion of these expressions did not improve the ability to fit the data or help to resolve inconsistencies in the values of the parameters obtained from those fits.

It is clear that the one-dimensional Ising model, even with corrections for canting and interchain exchange, is less able to describe FeTAC than CoTAC. The deviations from Ising-type behavior are much more severe in the case where the applied magnetic field is perpendicular to the easy axis. We are sure that the explanation for this failure does not arise from the interchain exchange, since such effects should clearly be less important for FeTAC than CoTAC. It appears to be more a problem of describing the magnetic behavior of a ferrous ion with an Ising model.

There have been several previous single-crystal studies of Fe^{2+} linear chain compounds where, as in FeTAC, the iron ion lies at the center of a distorted octahedron;[20–23,44] the most carefully studied include $RbFeCl_3 \cdot 2H_2O$ and $CsFeCl_3 \cdot 2H_2O$. These studies have involved spin cluster resonance, nuclear magnetic resonance, neutron diffraction, heat capacity, magnetization, and magnetic susceptibility;[20–23] there is notably little single-crystal magnetic susceptibility data reported. The low dimensionality of $RbFeCl_3 \cdot 2H_2O$ was demonstrated by heat capacity data[20] which is well described by the rectangular Ising model with a ratio $J'/J = 0.02$; this degree of isolation is comparable to that found in CoTAC. However, in describing the susceptibility data, the Ising model has not been used at all. A model in the full spin $S = 2$ representation which includes axial and orthorhombic crystal field splitting parameters has been used[22] to describe the high (50–300 K) and the low (1.2–4.2 K) temperature susceptibility data. There has been no report of the intermediate-temperature susceptibility data (12–50 K) which lie above the critical temperature of 11.96 K; this region might be expected to lend itself to a description by a simple 1D Ising model, considering that the first excited state lies 59 K above the pseudo-ground-state doublet.[22]

One final point of interest concerning the perpendicular susceptibilities is the small but rapid rise in both perpendicular susceptibilities χ_a and χ_c just below T_c (Figs. 5 and 13). In both cases, an increase of approximately 50% is seen as the temperature is lowered from 3 to 2 K. Below 2 K both χ_a and χ_c reach a constant value, showing almost no change to 1.4 K. Consider this feature in light of the Onsager model. At T_c the system orders in an arrangement of decoupled antiferromagnetic layers. The net exchange between the layers is zero by symmetry. This is a metastable state in which any shift in the structure to a lower symmetry would result in a more stable arrangement and a net nonzero interplane exchange. The brief but rapid rise in χ_a and χ_c just below T_c may indicate the occurrence of such a structural change. This sort of symmetry breaking is known to occur at the Neél temperature of transition metal oxides, such as NiO.[45]

E. Summary and conclusions

FeTAC can be modeled as a 1D Ising system with some restrictions; the Ising model is appropriate below approximately 20 K while deviations from the purely one-dimensional character occur below 6 K. The susceptibilities perpendicular to the bulk easy axis cannot be described with the same parameters used to describe $\chi_\parallel$. In comparison, the Ising model successfully describes all the susceptibility data for CoTAC up to 40 K. The relatively large J and small J' indicate that the ferromagnetic chains in FeTAC are a factor of 10 more isolated than that of CoTAC, making FeTAC the most one-dimensional system in the TAC series.

The magnetic structures of FeTAC and CoTAC are significantly different. In FeTAC the b axis is the bulk easy axis, although the local anisotropy fields are alternately canted with components along both c and a; in CoTAC the c axis is the bulk easy axis with all spins canted towards a, creating a weak ferromagnet. Finally, in the ordered state CoTAC is a 3D system of ferromagnetic layers ordered antiferromagnetically. An unambiguous assessment of the signs of the interchain exchange con-

stants is not available for FeTAC but a plausible model consists of 2D antiferromagnetic layers decoupled from each other by the the crystallographic symmetry, making FeTAC a true rectangular Ising magnet.

ACKNOWLEDGMENTS

This research was supported in part by the National Science Foundation (NSF), Division of Materials Research, Grant Nos. 8306432 (C.P.L.) and 8313710 (W.M.R.). The magnetometer was purchased with a grant from the NSF College Research Instrumentation Program. The Francis Bitter National Magnet Laboratory is supported by the National Science Foundation. We thank Roger D. Willett for the crystal structure determination; his work was supported in part by National Science Foundation Grant No. CHE-8408407. The x-ray diffractometer system was purchased with a grant from the Boeing Company.

---

*Present address: Laboratoire de Physique des Solides, Bâtiment 510, Université Paris-Sud, 91405 Orsay, France.

[1]S. Merchant, J. N. McElearney, G. E. Shankle, and R. L. Carlin, Physica **78**, 308 (1974).

[2]P. R. Newman, J. A. Cowen, and R. D. Spence, in *Magnetism and Magnetic Materials—1973 (Boston),* Proceedings of the 19th Annual Conference on Magnetism and Magnetic Materials, AIP Conf. Proc. No. 18, edited by C. D. Graham and J. J. Rhyne (AIP, New York, 1974), p. 391.

[3]K. Iio, M. Isobe, and K. Nagata, J. Phys. Soc. Jpn. **38**, 1212 (1975).

[4]I. Yamamoto and K. Nagata, J. Phys. Soc. Jpn. **43**, 1581 (1977).

[5]I. Yamamoto, K. Iio, and K. Nagata, J. Phys. Soc. Jpn. **49**, 1756 (1980).

[6]K. Takeda, T. Koike, I. Harada, and T. Tonegawa, J. Phys. Soc. Jpn. **51**, 85 (1982).

[7]R. E. Caputo, R. D. Willett, and J. A. Muir, Acta Crystallogr. **B32**, 2639 (1976).

[8]D. B. Losee, J. N. McElearney, G. E. Shankle, R. L. Carlin, P. J. Cresswell, and W. T. Robinson, Phys. Rev. B **8**, 2185 (1973).

[9]H. A. Groenendijk and A. J. van Duyneveldt, Physica **115B**, 42 (1982).

[10]R. D. Spence and A. C. Botterman, Phys. Rev. B **9**, 2993 (1974).

[11]S. O'Brien, R. M. Gaura, C. P. Landee, and R. D. Willett, Solid State Commun. **39**, 1333 (1981).

[12]R. Hoogerbeets, S. A. J. Wiegers, A. J. van Duyneveldt, R. D. Willett, and U. Geiser, Physica **125B**, 135 (1984).

[13]C. R. Stirrat, S. Dudzinski, A. H. Owens, and J. A. Cowen, Phys. Rev. B **9**, 2183 (1974).

[14]H. A. Algra, L. J. de Jongh, H. W. J. Blöte, and W. J. Huiskamp, Physica **78**, 314 (1974).

[15]H. A. Algra, L. J. de Jongh, W. J. Huiskamp, and R. L. Carlin, Physica **92B**, 187 (1977).

[16]D. B. Losee, J. N. McElearney, A. Siegel, R. L. Carlin, A. A. Khan, J. P. Roux, and W. J. James, Phys. Rev. B **6**, 4342 (1972).

[17]C. P. Landee, R. E. Greeney, W. M. Reiff, J. H. Zhang, J. Chalupa, and M. A. Navotny, J. Appl. Phys. **57**, 3343 (1985).

[18]J. D. Johnson and J. C. Bonner, Phys. Rev. B **22**, 251 (1980).

[19]D. N. Haines and J. E. Drumheller, J. Magn. Magn. Mater. **54-57**, 1145 (1986); D. N. Haines, K. Ruvindran, and J. E. Drumheller, Proceedings of the International Conference on Magnetism, Paris, 1988 [J. Phys. (Paris) (to be published)].

[20]K. Kopinga, Q. A. G. van Vlimmeren, A. L. M. Bongaarts, and W. J. M. de Jonge, Physica **86-88B**, 671 (1977).

[21]J. A. J. Basten, Q. A. G. van Vlimmeren, and W. J. M. de Jonge, Phys. Rev. B **18**, 2179 (1978).

[22]Q. A. G. van Vlimmeren, Ph.D. thesis, Eindhoven University of Technology, 1979.

[23]K. Kopinga, M. Steiner, and W. J. M. de Jonge, J. Phys. C **18**, 3511 (1985).

[24]Galbraith Laboratories, Knoxville, TN.

[25]C. F. Campana, D. F. Shephard, and W. M. Litchman, Inorg. Chem. **20**, 4039 (1981).

[26]G. Sheldrick, SHELXTL, Nicolet Analytical Instruments, Madison, WI, 1984.

[27]C. P. Landee, R. E. Greeney, and A. C. Lamas, Rev. Sci. Instrum. **58**, 1957 (1987).

[28]The ordering temperature was initially reported to be 3.25 K in Ref. 17. The difference value now reported reflects both more careful measurements and a slight shift in our temperature scale.

[29]J. M. Kincaid and E. G. D. Cohen, Phys. Rep. **22**, 57 (1975).

[30]R. E. Greeney, Ph.D. dissertation, Clark University, 1988.

[31]C. E. Johnson, Proc. Phys. Soc. London **88**, 943 (1966).

[32]S. Chandra and G. R. Hoy, Phys. Lett. **22**, 254 (1966).

[33]R. Ingalls, Phys. Rev. **128**, 1155 (1962).

[34]R. C. Thiel, H. DeGraff, and L. J. De Jongh, Phys. Rev. Lett. **47**, 1415 (1981).

[35]N. N. Greenwood and T. C. Gibb, *Mössbauer Spectroscopy* (Chapman & Hall, London, 1971).

[36]M. F. Thomas and C. E. Johnson, in *Mössbauer Spectroscopy,* edited by D. P. E. Dickson and F. J. Berry (Cambridge University Press, Cambridge, 1986), p. 179.

[37]B. Morosin and E. J. Graeber, J. Chem. Phys. **42**, 898 (1963).

[38]A. Narath, Phys. Rev. **139**, A1221 (1965).

[39]J. Chalupa and M. R. Giri, Solid State Commun. **29**, 313 (1979).

[40]M. E. Fisher, J. Math. Phys. **4**, 124 (1963).

[41]R. L. Carlin and A. J. van Duyneveldt, *Magnetic Properties of Transition Metal Compounds* (Springer-Verlag, New York, 1977).

[42]L. Onsager, Phys. Rev. **65**, 117 (1944).

[43]J. Chalupa and M. A. Navotny, Solid State Commun. **54**, 843 (1985).

[44]J. Y. Chen, S. Simizu, and S. A. Friedberg, J. Appl. Phys. **57**, 3338 (1985).

[45]D. H. Martin, *Magnetism in Solids* (Iliffe, London, 1967), p. 56.